NRC Publications Archive
Archives des publications du CNRC

Infrared spectroscopy on size-controlled synthesized Pt-based nano-catalysts
Baranova, E. A.; Bock, C.; Ilin, D.; Wang, D.; MacDougall, B.

NRC Publications Record / Notice d'Archives des publications de CNRC:
https://nrc-publications.canada.ca/eng/view/object/?id=6769273a-3bd9-4aa5-b04f-8abbf857f304
https://publications-cnrc.canada.ca/fra/voir/objet/?id=6769273a-3bd9-4aa5-b04f-8abbf857f304

National Research
Council Canada

Conseil national de
recherches Canada

Canada

Infrared spectroscopy on size-controlled synthesized Pt-based nano-catalysts

E.A. Baranova, C. Bock *, D. Ilin, D. Wang, B. MacDougall

National Research Council of Canada, Institute for Chemical Process and Environmental Technologies,
Montreal Road, Ottawa, ON, Canada K1A 0R6

Abstract

Pt, Ru and Pt/Ru nano-particles, synthesized in ethylene glycol solutions, are studied using infrared (IR) spectroscopy and high resolution transmission electron microscopy (HRTEM). The synthesis method allows the control of the mono- and bi-metallic catalyst particle sizes between 1 and 5.5 nm. The IR spectra of CO adsorbed (CO_{ads}) on the Pt, Ru and bi-metallic Pt/Ru colloids are recorded as a function of the particle size. The stretching frequency of CO_{ads} depends on the particle size and composition. Strong IR bands due to the stretching vibration of CO_{ads} are observed between 2010 and 2050 cm^{-1} for the Pt nano-particles, while two IR bands between 2030 and 2060 cm^{-1} for linear bonded CO_{ads}, and at lower wavenumbers between 1950 and 1980 cm^{-1} for bridged bonded CO_{ads}, are found for the Ru particles. The IR spectra for the Pt/Ru nano-sized catalyst particles show complex behaviour. For the larger particles ($>2 \pm 0.5$ nm), two IR bands representative of CO_{ads} on Ru and Pt–Ru alloy phases, are observed in the range of 1970–2050 cm^{-1}. A decrease in the particle size results in the appearance of a third band at ~2020 cm^{-1}, indicative of CO_{ads} on Pt. The relative intensity of the band for CO_{ads} on the Pt–Ru alloy vs. the Pt phase decreases with decreasing particle size. These results suggest that Ru is partially dissolved in the Pt lattice for the larger Pt/Ru nano-particles and that a separate Ru phase is also present. A Pt–Ru alloy and Ru phase is observed for all Pt/Ru particles prepared in this work. However, a decrease in particle size results in a decrease of the number of Pt and Ru atoms in the Pt–Ru alloy phase, as they are increasingly present as single Pt and Ru phases.
© 2006 Elsevier B.V. All rights reserved.

Keywords: Infrared absorption spectroscopy; Platinum; Ruthenium; Carbon monoxide; Pt–Ru alloys; Surface structure; Catalysis

1. Introduction

Small metal particles in the nanometer range display chemical and physical properties different from bulk materials and play an important role in heterogeneous catalysis [1,2]. The reactivity of nano-sized catalyst particles is associated with their high ratio of surface to bulk atoms. Nano-sized Pt/Ru catalysts are of major interest as anode catalysts for direct methanol and reformate fuel cells [3,4]. CO adsorbed (CO_{ads}) on the catalyst surface is produced as a result of the electro-oxidation reaction of methanol, and its oxidation to CO_2 is a critical step. Therefore, CO is often used as a

test molecule to study Pt and Pt/Ru catalysts. The size effect of catalyst nano-particles on the electro-catalytic oxidation reaction of adsorbed CO has been reported previously [5]. Much interest has also been devoted to the synthesis of Pt/Ru catalysts [2,5–8]. Despite the various methods tested for the preparation of nano-sized catalysts, an effective control of particle size and composition, and subsequent full characterization of these catalysts, is still a challenge.

Recently, a rapid and simple synthesis method for the preparation of Pt/Ru colloids of controlled size (0.7–4 nm), and their subsequent deposition on high surface area carbons, has been developed [9]. This method is based on the well-known polyol synthesis method, which has been previously applied to the synthesis of unsupported Pt/Ru powder catalysts [10] and mono-metallic Pt and

* Corresponding author. Tel.: +1 613 990 2252; fax: +1 613 991 2384.
E-mail address: christina.bock@nrc-cnrc.gc.ca (C. Bock).

Ru nano-particles [11]. This method is proposed to involve glycolate as a stabilizer for these Pt-based colloids. Glycolate is a simple organic molecule that can be oxidatively removed by heat treatment in air at temperatures as low as 160 °C. The use of low temperatures is important to avoid temperature induced alterations of the Pt/Ru catalyst composition, in particular Pt surface segregation [10]. Catalytic studies showed that particular Pt/Ru catalysts prepared using the ethylene glycol method display better CH_3OH electro-oxidation activities than commercial catalysts [9]. This synthetic method, which is easy to scale up and is very reproducible, has the potential to generate very active catalysts. In previous work [9], the Pt/Ru catalysts prepared using this method were characterized using transmission electron microscopy (TEM) and slow scan X-ray diffraction spectroscopy (XRD). Based on the XRD results, it is believed that the particles are partially alloyed and that a separate Ru phase exists. Smaller particles are not alloyed, as alloy formation for particles of less than 1 nm diameter is not achievable. This is due to the largely different surface energies of Pt and Ru and the fact that for smaller particles the majority of the atoms are surface atoms [9]. It is clear that the synthesis method needs to be improved to yield higher degrees of Pt–Ru alloying and full characterization, including information about the surface structure and composition of these nano-particles, is needed. Very few experimental studies deal with the surface structure of Pt/Ru nano-particles [7,13,14]. The reason is the complexity of bi-metallic structure and the lack of proper and readily available surface characterization tools for nano-particles [2]. Infrared (IR) spectra of CO_{ads} are frequently used to probe the surface structure of nano-sized catalysts [14–16]. A number of these studies have been carried out in solutions where the catalyst is simply present in the colloidal form [12]. The study of the vibrational CO_{ads} spectra of colloidal catalyst solutions offers several advantages, one of them is the possibility of investigating the catalyst-metal structure without the influence of the support, which can significantly alter the electronic properties of the electrocatalyst due to metal-support interaction effects [14,17].

In the present work, the use of the CO_{ads} IR spectra to characterize the surface structure of Pt/Ru nano-particles is investigated. Pt, Ru and Pt/Ru colloids of various sizes are synthesized and the influence of catalyst particle size and composition on the IR stretching frequency is studied. The *in-house* prepared catalysts are also characterized using high resolution transmission electron microscopy (HRTEM). The preparation and characteristics of the mono-metallic Pt and Ru-colloids are investigated and discussed, followed by the more complex Pt/Ru system.

2. Experimental

2.1. Preparation of Pt, Ru and bi-metallic Pt/Ru colloids

The details of the synthesis of the colloidal solutions can be found elsewhere [9]. The synthesis of the Pt, Ru and Pt/ Ru colloids was carried out in ethylene glycol (Anachemia, ACS grade) solutions containing different concentrations of sodium hydroxide (EM Science, ACS grade).

2.1.1. Pt colloids

0.4652 g of $PtCl_4$ (Alfa Aesar, 99.9% metals basis) was dissolved in 50 mL of ethylene glycol containing between 0.2 and 0.1 M NaOH. The solutions were stirred for 30 min, subsequently heated and refluxed for 3 h at 160 °C. Dark brown solutions containing Pt colloids were formed rapidly (<15 min) in this manner and are referred to as "Pt colloidal solutions".

2.1.2. Ru colloids

Ru colloids were prepared by following the same procedure as for the Pt colloids, but using 0.2766 g of $RuCl_3$ (Alfa Aesar, 99.9% metals basis) and NaOH concentration between 0.15 and 0.05 M. The resulting dark brown solutions containing Ru colloids are referred to as "Ru colloidal solutions".

2.1.3. Pt/Ru colloids

These colloids were prepared following essentially the same procedure as used for the mono-metallic colloids, however, using 0.2326 g of $PtCl_4$ and 0.1383 g of $RuCl_3$. The NaOH concentrations of the synthesis solutions varied between 0.12 and 0.06 M. The resulting solutions containing the Pt/Ru colloids are referred as "Pt/Ru colloidal solutions".

The pH of the final, synthesis solution was measured using pH paper and is referred to as "synthesis solution pH" in this work. All colloidal solutions were stored in air and were found to be stable for at least 6 month, as indicated in the unchanged IR characteristics of the CO_{ads} bands for a particular colloidal solution.

2.2. Instrumentations/techniques

2.2.1. TEM

The TEM samples were prepared by suspending the particle solution in methanol followed by sonication for several minutes. One drop of the dilute suspension was placed onto a 300 mesh carbon-coated holey TEM copper grid and was dried in air. The dried grid was then loaded into a double tilt sample holder. The sample was then examined with a Philips CM20 STEM equipped with a Gatan UltraScan 1000 CCD camera combined with a Digital Micrograph Software (dm3.4) and an energy dispersive X-ray spectrometer: INCA Energy TEM 200. TEM images were taken at 200 kV. Size distributions of a particular colloid were obtained by counting at least 100 particles. For the high resolution studies, the samples were prepared following the same procedure as for the TEM. The samples were examined with a JEOL, JEM-2100 F HRTEM equipped with a field emission gun. HRTEM images were taken at 200 kV. Metal–metal distances were measured from HRTEM images measuring the distance of at least

five particles of a particular colloid. The TEM was calibrated by utilizing a lattice image of graphite carbon as a standard in the high resolution range. Measurements on the lattice images of the particles were realized by profiling the lattice planes using the Digital Micrograph Software.

2.2.2. IR

A Brucker IFS 66/S FTIR spectrometer equipped with a globar IR source and a narrow-band mercury-cadmium-telluride (MCT) detector was used. The latter was cooled using liquid nitrogen. A single reflection MIRacle Si crystal, with a 2 mm diameter of exposed area (PIKE Technologies), was used in this work. The Si ATR crystal has an incident angle of ∼43°. Before and during the IR measurements, the sample compartment was flushed with compressed air. Samples were prepared by placing a 10 µL drop of the colloidal metal solution (i.e., 27 µg of Pt and 13 µg of Ru) on the crystal, followed by drying at 80 °C in air for 30 min. Single beam spectra were obtained by averaging 32 scans with a 1.5 cm^{-1} resolution and a scan speed of 20 kHz. The absorbance spectra were calculated automatically using an OPUS software program (Bruker) that uses the following relationship:

$$Absorbance = -\log(R/R_0) \times x/1000 \qquad (1)$$

In Eq. (1), R is the intensity of the sample spectrum, R_0 is the intensity of the reference spectrum, and x represents the wavenumber. Reference spectrum is taken on the clean crystal (in the absence of colloids). The penetration depth of IR light into the sample depends on the wavenumber, and hence, $x = 1000$ is used to compensate for the contribution of the different penetration depths with the wavenumber.

3. Results and discussion

First the CO$_{ads}$ IR spectra and TEM results for the Pt and Ru colloids are discussed. This is followed by the investigation and discussion of the Pt/Ru colloids. The results from the IR (CO$_{ads}$ bands and assignments) and HRTEM studies obtained in this work are summarized in Tables 1 and 2.

3.1. Mono-metallic Pt and Ru colloids

Mono-metallic Pt and Ru colloids of a range of different sizes were synthesized in this work using the ethylene glycol method [9]. In all cases, ethylene glycol served as a reducing agent. The size of the resulting mono-metallic particles can be well controlled by varying the pH of the synthesis

Table 2
Summary of HRTEM results

Colloids	Metal–metal distance, Å	Structure	Metal	hkl
Pt	2.265	fcc	Pt	(111)
Ru		hcp		
Pt/Ru	2.22	fcc	Pt–Ru alloy	(111)
	1.99[a]	fcc	Pt	(200)
		hcp	Ru	(101)
		fcc	Pt–Ru alloy	(200)

[a] Three possible structures.

Table 1
Summary of vibrational wavenumbers/cm^{-1} for CO adsorbed on mono- and bi-metallic colloids

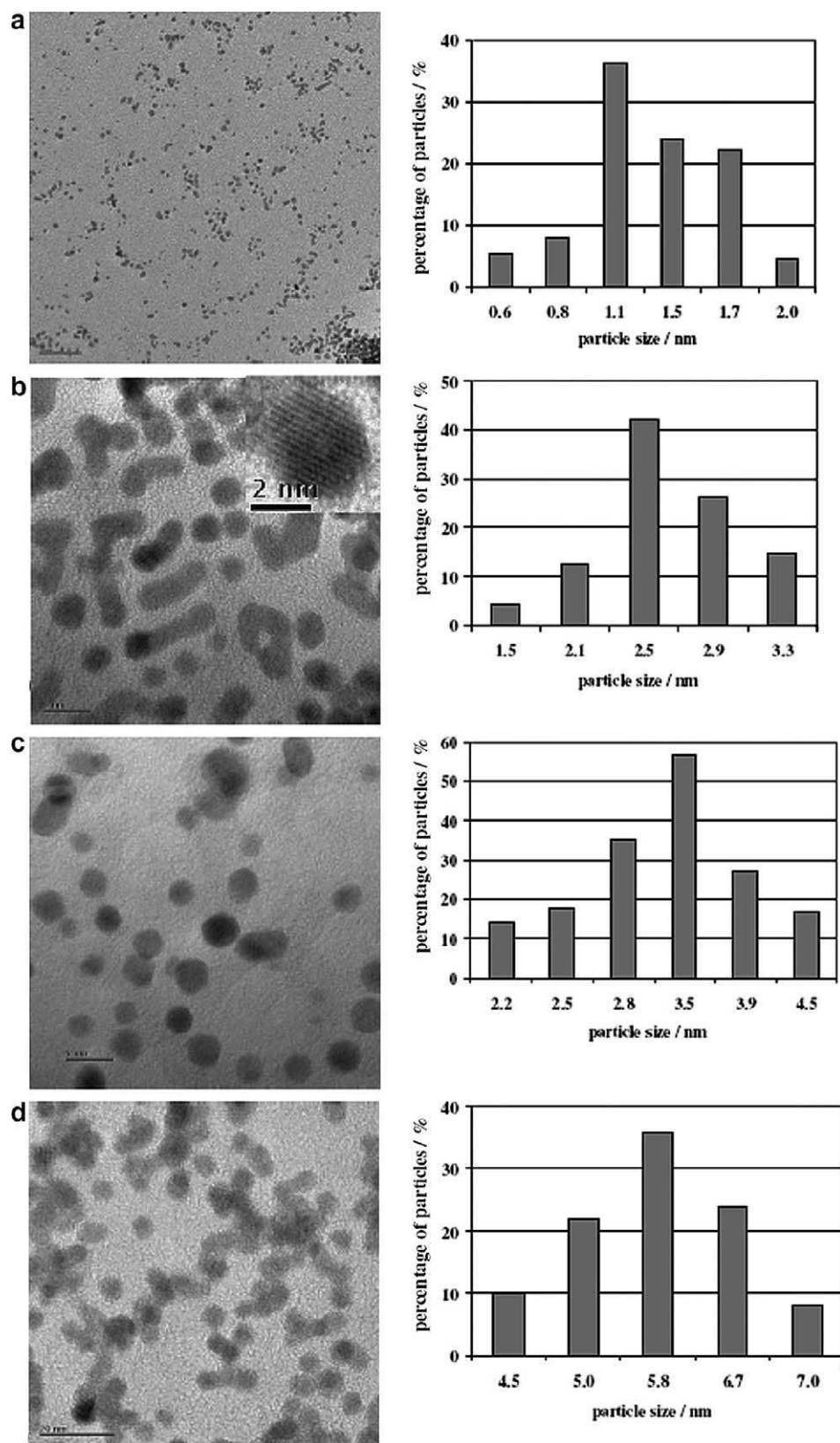| Colloids	Particle size, nm	vCO (linear)		vCO (bridged)		Comments
				2-fold	3-fold	
Pt	1 ± 0.5	2017 (Pt edge sites)	Shoulder at 2015 cm^{-1} due to CO$_{ads}$ on Pt edge sites			Red shift of vCO with decreasing particle size
	2.5 ± 0.5	2023 (Pt edge sites)				
	3 ± 0.8	2027 (Pt edge sites)				
	3.5 ± 1.0	2036 (Pt terrace sites)				
	4 ± 1.0	2042 (Pt terrace sites)				
	5.5 ± 1.5	2046 (Pt terrace sites)				
Ru	1 ± 0.5	2031		1955	1900	Red shift of vCO with decreasing particle size
	1.7 ± 0.8	2032		1958	1900	
	2.8 ± 1.0	2040		1969	1943	
	3.5 ± 1.5	2050		1980	1944	
	4 ± 1.5	2050		1975		
Pt/Ru	1 ± 0.5	2055 (Pt–Ru edge sites)	2013 (Pt edge sites)	1982	1941	Blue shift of vCO on Pt/Ru sites with decreasing particle size
	1.4 ± 0.5	2054 (Pt–Ru edge sites)	2019 (Pt edge sites)	1981	1942	
	1.6 ± 0.5	2053 (Pt–Ru edge sites)	2020 (Pt edge sites)	1980		
	2 ± 0.8	2052 (Pt–Ru edge sites)	2027 (Pt edge sites)	1978		
	2.2 ± 0.8	2051 (Pt–Ru edge sites)		1975		
	2.5 ± 1.0	2049 (Pt–Ru edge sites)		1975		
	3 ± 1.5	2048 (Pt–Ru edge sites)		1971		
	4 ± 1.5	2047 (Pt–Ru edge sites)		1970		

Fig. 1. TEM images (left) and corresponding histograms (right) of Pt colloids, synthesized in ethylene glycol solution using following NaOH concentrations: (a) 0.175 M (pH = 7); (b) 0.13 M (pH = 5); (c) 0.12 M (pH = 4.5); (d) 0.11 M (pH = 4). The bars in (b) and (c) indicate a 5 nm scale, and the bars in (a) and (d) indicate a 20 nm scale. The magnification of the images is (a) 135k× and (b)–(d) 580k×.

solution using different NaOH concentrations, as discussed previously [9]. The reaction of ethylene glycol with the noble metal precursor salts leads to the oxidation of ethylene glycol to aldehydes, which are not very stable and are easily oxidized to compounds such as glycolic and oxalic acid. Previous work has shown that the synthesis product, glycolic acid (or glycolate depending on the pH), is predominantly present in the synthesis solution. The electrons donated from these oxidation reactions result in the reduction of the Pt- and Ru-precursor salts. In alkaline solutions, glycolic acid is present in its de-pronotated, anionic form, i.e., glycolate, which is believed to act as a stabilizer for the colloids [9]. Ethylene glycol can also be oxidized via a hydrogen abstraction mechanism from the carbon atoms by Pt and Ru resulting in adsorbed CO (CO_{ads}) on the colloidal catalyst particles. It is well known that platinum is an excellent catalyst to abstract hydrogen from carbon atoms [18]. Ru also displays some activity for the hydrogen adsorption reaction [19].

3.1.1. TEM for Pt colloids

Fig. 1 shows examples of TEM images and the corresponding histograms for four Pt colloids synthesized in this work using different NaOH concentrations. The TEM images show that not only well defined, almost "spherical" but also "rod-like" Pt colloids are prepared using the ethylene glycol method. There is some degree of particle agglomeration that likely takes place over time. Nevertheless, the identity of individual particles is recognizable even for agglomerated particles. Pt particles with a mean size diameter of 1–6 nm were prepared depending on the synthesis solution pH. The full set of particle sizes, and their size distribution prepared in this work, are shown in
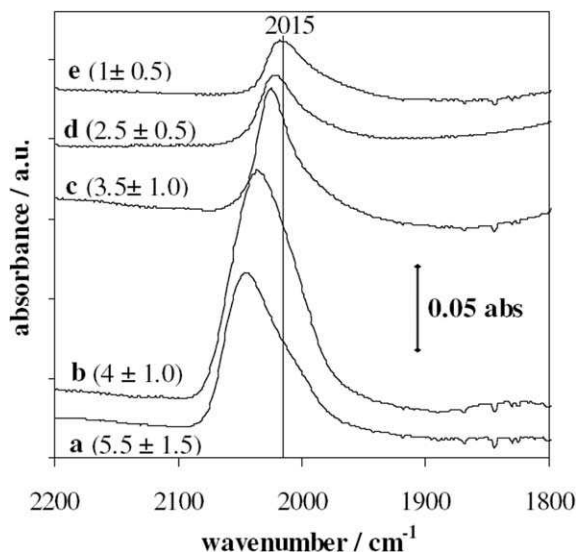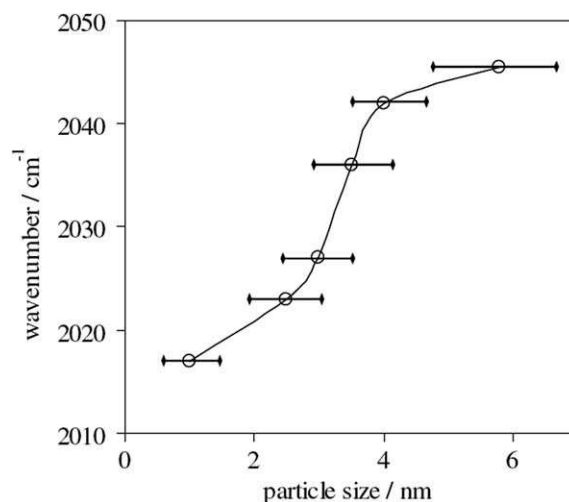

Fig. 3. Evolution of the CO_{ads} stretch frequency as a function of the Pt particle size. The horizontal lines indicate the particle size distribution.

Fig. 3. The smallest Pt particles, of 1 ± 0.5 nm diameter, were prepared using high NaOH concentrations. The particle size increases with decreasing pH of the synthesis solution consistent with the size control mechanism reported previously for bi-metallic Pt/Ru particles [9]. The platinum particles prepared in this work are of narrow size distribution, although the size distribution increases somewhat as larger particles are made. TEM images obtained at high resolution (see insert in Fig. 1b) reveal the structure of the Pt particle to be face-centered cubic (fcc) with a metal to metal distance of 2.26 Å. This value corresponds to metallic Pt (2.265 Å) with (1 1 1) crystal orientation [20]. It is interesting to note that single as well as twin particles were obtained by this method, although single particles were dominantly present. These results are consistent with previously reported characteristics of Pt nano-particles, for which a fcc cubo-octahedral form has been suggested, based on extended X-ray adsorption fine structure (EXAFS) analyses [21]. The cubo-octahedral form is also the thermodynamic stable form of small Pt particles, according to theoretical studies [22]. Therefore, the Pt nano-particles prepared in this work are possibly also cubo-octahedral.

3.1.2. IR for Pt colloids

Fig. 2 shows the IR spectra of CO_{ads} recorded for freshly prepared Pt colloids. The CO_{ads} is present as a result of the synthesis reaction, as discussed above. A pronounced vibrational band is observed at frequencies between 2010 and 2050 cm^{-1}, depending on the Pt particle size. This frequency range is normally assigned to the stretching vibration of CO_{ads} in an on-top configuration on Pt [14]. It should be noted that the positions of the CO_{ads} bands were found to be independent of the pH of the synthesis solution once the nano-particles were formed, i.e., the amount of NaOH in the final colloidal solutions did not influence the CO_{ads} band. The CO_{ads} stretching frequency ($\nu_{CO_{ads}}$) shifts gradually to lower wavenumbers with

Fig. 2. IR spectra of Pt colloids different size synthesized in ethylene glycol at different pH's: (a) 5.5 ± 1.5 nm (pH = 4); (b) 4 ± 1.0 nm (pH = 4.5); (c) 3.5 ± 1.0 nm (pH = 5); (d) 2.5 ± 0.5 nm (pH = 6); (e) 1.0 ± 0.5 nm (pH = 7). The resulting particle sizes in nm are also indicated in the figure.
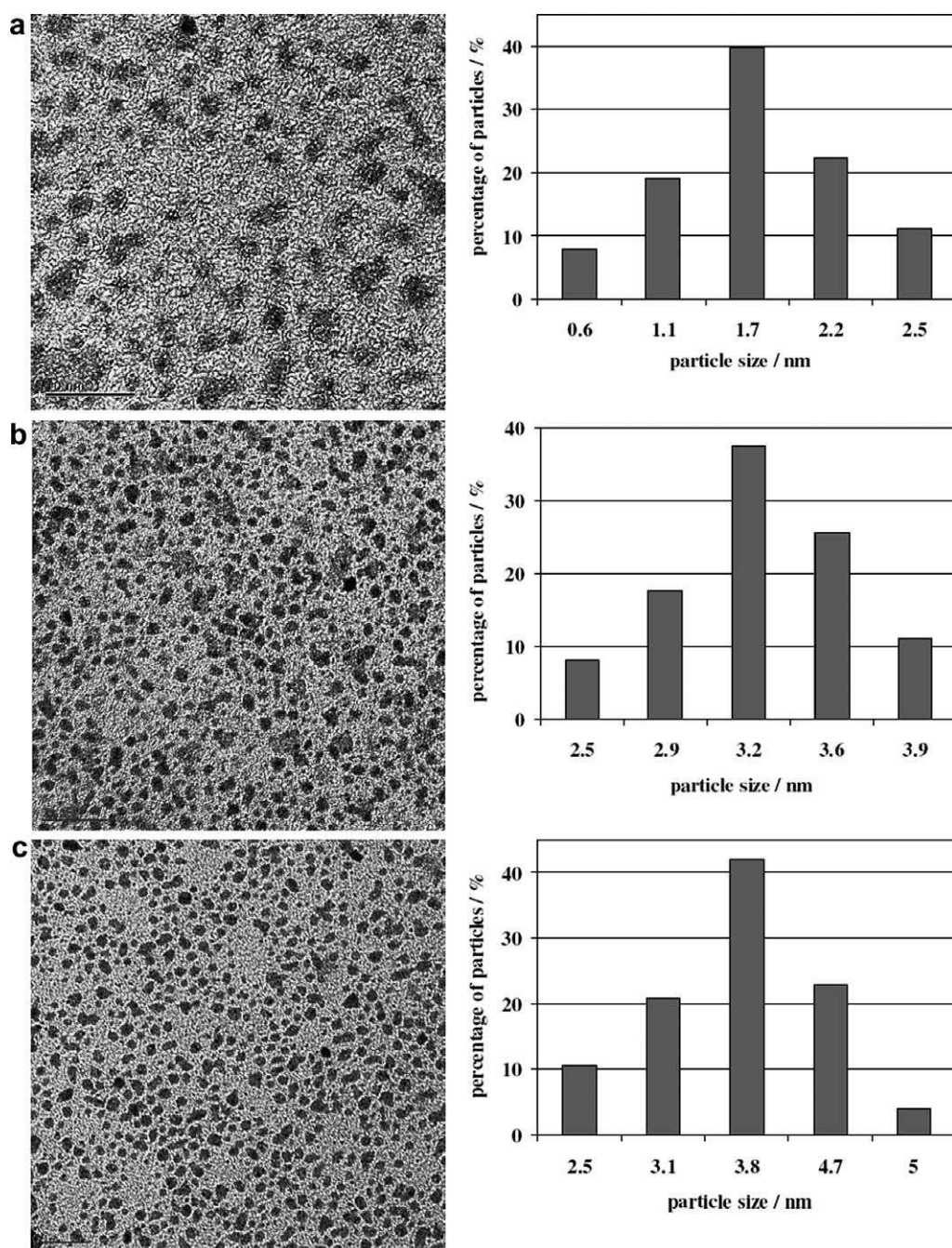
Fig. 4. TEM images (left) and corresponding histograms (right) of Ru colloids, synthesized in ethylene glycol solution using following NaOH concentrations: (a) 0.13 M (pH 8); (b) 0.11 M (pH 7); (c) 0.08 M (pH 5). The bar in (a) indicates a 5 nm scale, and the bars in (b) and (c) indicate a 20 nm scale. The magnification of the images is (a) 380k×, (b) 175k× and (c) 230k×.

a decrease in the Pt particle size, as shown in Fig. 3. A shift of about 29 cm^{-1} of the CO$_{ads}$ peak to higher wavenumbers with increasing intensity is observed for the Pt particles that increase in size from 1 to 5.5 nm. Furthermore, the peak for the larger particles is asymmetrical. In fact for the two largest particles, a shoulder with a maximum at ca. 2015 cm^{-1}, i.e., at essentially the same position as observed for the small (1 nm) Pt particles, is recognizable.

Consistent with Park et al. [23], the $\nu_{CO_{ads}}$ value (in the 2040 cm^{-1} range) of the larger particles is assigned to ter-

race Pt(1 1 1) sites, while the CO$_{ads}$ band at the lower frequencies (in the 2015 cm^{-1} frequency range) observed for the smaller particles, as well as the shoulder for the larger particles, is assigned to reflect CO adsorbed on edge Pt sites. CO is more strongly adsorbed on the edge vs. the terrace sites, hence, the lower ν_{CO} value is believed to reflect the higher binding energy of CO on the edge vs. the terrace sites. The ratio of Pt atoms located on the terrace vs. edge sites decreases with decreasing particle size [21]. Therefore, the intensity of the vibration band for CO$_{ads}$ on edge

($\sim$2015 cm^{-1}), vs. the band for CO$_{ads}$ on terrace sites ($\sim$2040 cm^{-1}), is predicted to increase with decreasing particle size, as experimentally observed (Fig. 2). For particles of 1 nm diameter, essentially all Pt atoms are located at the edges, as the particle size is too small for terraces to form and only the vibration band for CO$_{ads}$ on edge sites is observed.

In the present work, the larger particles (>3.5–5.5 nm) exhibit high vibrational frequencies (2042 cm^{-1}) but show deviation from the value for bulk Pt(111). Reported $\nu_{CO_{ads}}$ values for bulk Pt(111) are 2066 cm^{-1} [24] and 2090 cm^{-1} [25]. The former value is observed in 0.1 M HClO$_4$ solutions under potential control and for a CO coverage (θ_{CO}) of 60%. It has been reported that the CO coverage influences the $\nu_{CO_{ads}}$ value. Furthermore, the potential and presence of the electrolyte solution also influence the $\nu_{CO_{ads}}$ value and are possibly responsible for the observed differences. The higher frequency value of 2090 cm^{-1} is reported for low θ_{CO} on Pt(111) in ultra-high vacuum (UHV), thus further emphasizing the difference between bulk Pt(111) and the nano-particles studied here. The CO coverage is unknown for the particles studied in this work. A "saturated" CO coverage seems to have been reached, as indicated by the fact that no further CO could be adsorbed by bubbling CO through the colloidal solutions. However, the θ_{CO} value could be a function of the particle size and composition.

3.1.3. TEM for Ru colloids

Typical examples of TEM images for three particular Ru colloids prepared in this work are shown in Fig. 4. It is seen that the Ru nano-particles synthesized in this work are well dispersed. Similar to the Pt colloids, they also display a narrow size distribution, as shown in the histograms in Fig. 4. Measurements of the particle size by TEM indicate a dependence of the particle size on the synthesis solution pH. Ru particles are between 1 and 4 nm in size, as shown in Fig. 5. However, the shape of the Ru colloids is different from the well-defined shape observed for the Pt particles. The Ru particles are much less regular than the Pt nano-particles and the surface of the Ru particles is made of a large number of corners and edges. Also, the TEM images suggest that the Ru nano-particles have a tendency to agglomerate. This makes it more difficult to obtain high resolution images of the same quality as those for the Pt colloids. The Ru particles observed in HRTEM display a hexagonal-closed-packed (hcp) structure.

3.1.4. IR for Ru colloids

Fig. 5 shows the IR spectra for the ruthenium particles, in the region of the CO$_{ads}$ stretching frequencies. Two bands are observed for all the ruthenium particles prepared in this work. The band typical for linear bonded CO$_{ads}$ is observed between 2030 and 2060 cm^{-1} and a band for 2-fold bridged bonded CO$_{ads}$ (Ru(CO)Ru) is observed at lower wavenumbers between 1950 and 1980 cm^{-1} [14,26]. Similar results are reported for Ru colloids stabilized using
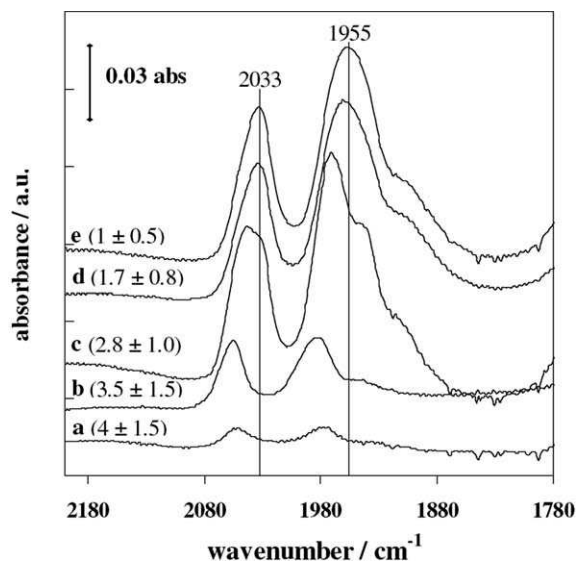

Fig. 5. IR spectra of Ru colloids of different size synthesized in ethylene glycol at different pH's: (a) 4 ± 1.5 nm (pH = 4.5); (b) 3.5 ± 1.5 nm (pH = 5); (c) 2.8 ± 1 nm (pH = 6); (d) 1.7 ± 0.8 nm (pH = 7); (e) 1.0 ± 0.5 nm (pH = 7.5). The resulting particle sizes in nm are also indicated in the figure.

nitrocellulose and cellulose acetate [27]. Those authors observed two adsorption bands in the 2050–1950 cm^{-1} region and a band localized at 1968 cm^{-1} was assigned to a CO molecule adsorbed in a bridging mode.

The IR spectra for the Ru particles show a dependence on particle size, as was similarly observed for the platinum particles. Again, the ν_{CO} shifts to lower values with decreasing particle size, which may indicate a stronger CO bonding to the surface of the smaller particles and/or differences in the CO coverage for particles of different size. Furthermore, as seen in Fig. 5, the ratio of the band inten-
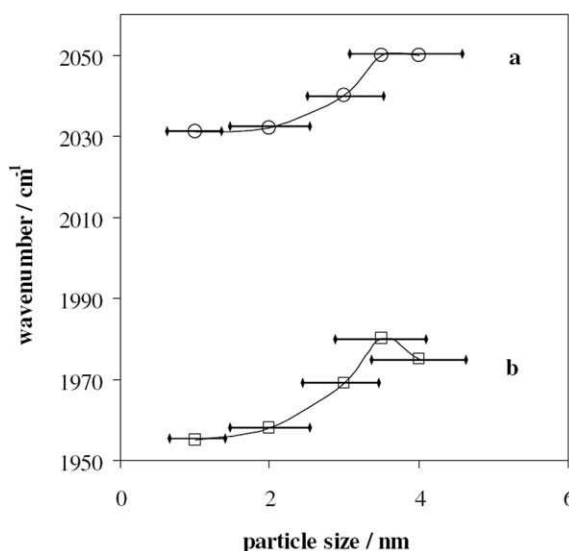

Fig. 6. Evolution of the CO$_{ads}$ stretch frequencies as a function of the Ru particle size. (a) linearly bonded CO; (b) 2-fold bridged bonded CO. The horizontal lines indicate the particle size distribution.

sity for linear CO (higher v_{CO} values) to bridging CO (lower v_{CO} values) decreases as the particle size decreases. An additional band, seen in the shoulder located at ca. 1920 cm^{-1}, appears and the band for bridged-bonded CO broadens with a decrease in particle size. This is possibly due to different crystallographic orientations of the Ru particles of different size. According to matrix-isolation studies by Hulse and Moskovits [28,29], designed to obtain IR bands from CO/metal complexes of formula M_nCO (M = metal, $n = 2, 3...$), the shoulder at 1920 cm^{-1} can be related to CO adsorption in 3-fold bridged mode. Those authors [28,29] assigned bands in the region of 1960 cm^{-1}

to 2-fold bridged CO molecules and in the 1930 cm^{-1} region to 3-fold bridged CO's [14]. The position of the peaks for linear and bridged CO shows a strong frequency downshift with decreasing particle size (Fig. 6) similar to the Pt nano-particles.

3.2. Bi-metallic Pt/Ru particles

3.2.1. TEM

Typical TEM images for three Pt/Ru colloids synthesized in this work are shown in Fig. 7. The particle size and distribution of the Pt/Ru nano-particles prepared in
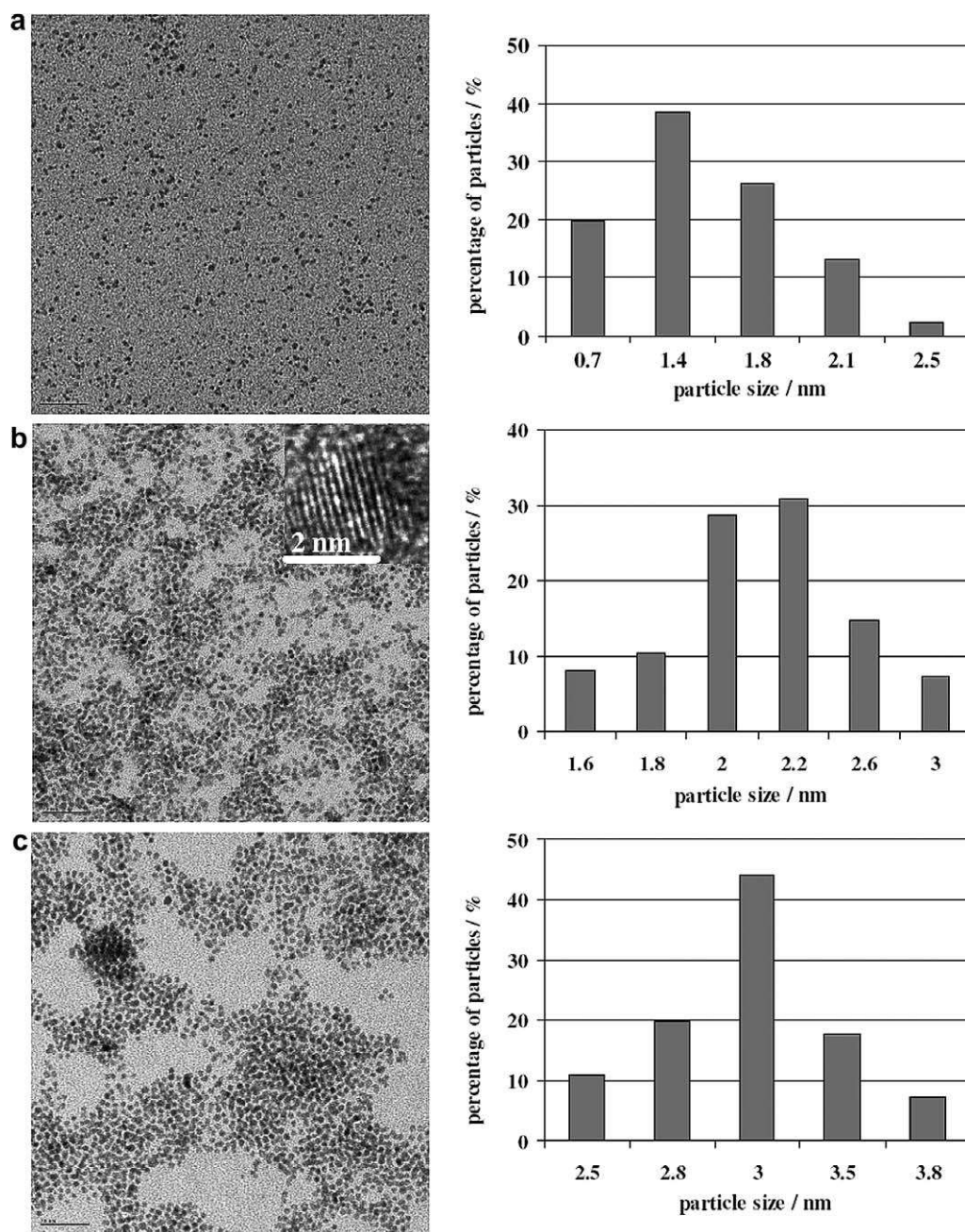

Fig. 7. TEM images (left) and corresponding histograms (right) of Pt/Ru colloids, synthesized in ethylene glycol using the following NaOH concentrations: (a) 0.11 M (pH 8); (b) 0.085 M (pH 7); (c) 0.08 M (pH 5). The bars indicate a 20 nm scale, corresponding to a magnification of 135k×.

this work are also shown in Fig. 7. The size of the Pt/Ru catalyst particles varies between 1 and 4 nm depending on the synthesis solution pH and the resulting particles display narrow size distribution similar to the results obtained in previous work [9]. HRTEM measurements conducted on large particles (2–4 nm) reveal the presence of two types of particles with different metal–metal distances. Calculated from HRTEM (Fig. 7b), the metal–metal distance of one type of particles is determined to be about 2.22 Å. This is lower than the value (2.265 Å) found for the Pt colloids, and hence, is believed to reflect Pt–Ru alloy formation. For the second type of particles, a metal–metal distance of 1.99 Å is measured from the HRTEM images. This may be Pt(200) or Ru(101) that have reported metal–metal distances of 1.9616 Å and 2.056 Å, respectively, or also a Pt–Ru alloy [20].

3.2.2. IR

The IR spectra for Pt/Ru particles show complex behaviour, as shown in Fig. 8. For the larger particles (>2 nm), two bands are observed in the frequency range of 1955–1985 and 2047–2057 cm^{-1}. The band observed at high wavenumbers (2047–2057 cm^{-1}) varies slightly with particle size. An increase in the v_{CO} value of this band with decreasing particle size is observed. This blue shift in frequency is opposite to the frequency-particle size shift observed for the mono-metallic Pt and Ru particles, where a decrease in the particle size leads to a decrease in the stretching frequency. This "new" band is assigned to a CO stretch on neighbouring Pt/Ru step sites. This assignment is based on results reported by Schlapka et al. [25]. They reported
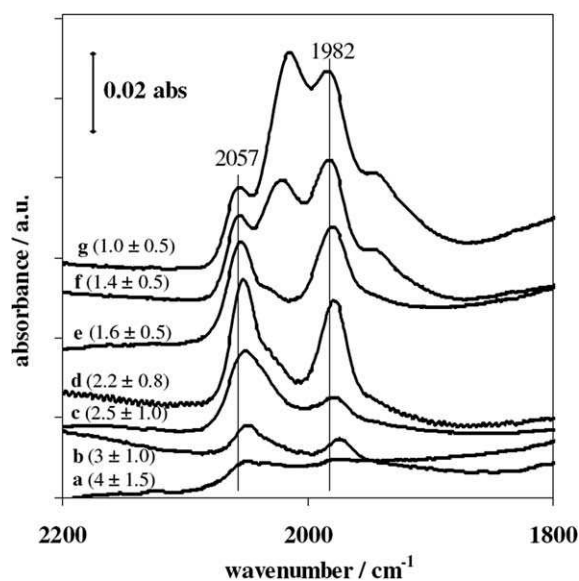

Fig. 8. IR spectra of Pt/Ru bi-metallic colloids of different size synthesized in ethylene glycol at different pH's: (a) 4.0 ± 1.5 nm (pH = 4); (b) 3.0 ± 1.0 nm (pH = 4.5); (c) 2.5 ± 1.0 nm (pH = 5); (d) 2.2 ± 0.8 nm (pH = 5.5); (e) 1.6 ± 0.5 nm (pH = 6); (f) 1.4 ± 0.5 nm (pH = 6.5); (g) 1.0 ± 0.5 nm (pH = 7). The resulting particle sizes in nm are also indicated in the figure.

v_{CO} values between 2033 and 2050 cm^{-1} for CO adsorbed on various Pt/Ru step sites. Furthermore, they related a decrease in the v_{CO} values to an increase in the size of the Pt islands formed on their Ru(0001) substrate. Therefore, the "apparent abnormal" blue shift in frequency with decreasing particle size may reflect more Pt "segregation" on the catalyst surface, giving rise to Pt "surface" clusters and a subsequent change in the Pt to Ru site distribution. This will have substantial implications for the "degree of alloying" on the surface; these very important factors will be the subject of future investigations.

The peak around 1982 cm^{-1} in Fig. 8 corresponds to CO adsorbed on Ru in a 2-fold bridge mode and the shoulder at 1930 cm^{-1} corresponds to a 3-fold bridged CO consistent with the assignments for the Ru only, i.e., Pt-free, particles (Fig. 5). This band, assigned to bridged CO, is observed for all synthesized Pt/Ru particles and is shifted to lower frequency values with increasing particle size, i.e., showing a particle size behaviour as similarly observed for the mono-metallic Pt and Ru colloids. The presence of an IR band for CO$_{ads}$ on Ru suggests that Ru is only partially dissolved into the Pt fcc lattice, i.e., a separate Ru phase exists next to the Pt–Ru alloy phase. Furthermore, it is seen in Fig. 8 that a decrease in the particle size leads to the appearance of a third band located between 2013 and 2020 cm^{-1}. The intensity of this band increases as the particle size decreases and becomes clearly visible for particles of less than 2 nm size. The position of this band is very similar to the frequency observed for CO adsorbed a-top on Pt sites (Fig. 5). Therefore, the smaller particles are believed to consist of a mixture of separate Pt and Ru phases as well as Pt–Ru alloy particles. Furthermore, the fact that the relative intensity of the CO band for both the Ru and Pt sites vs. the Pt–Ru alloy sites gradually increases with decreasing particle size could suggest that the ratio of atoms in the Ru and Pt phases vs. the Pt–Ru alloy phase increases as the particle size decreases. Such behaviour is indeed expected, since for the smaller particles an increasing number of less than 1 nm particles are present. As discussed in previous work [9], more than 80% of the atoms are "on the surface" for less than 1 nm Pt and Ru particles, and Pt–Ru alloy formation is not predicted to take place in such particles.

4. Conclusion

Infrared (IR) spectroscopy and high resolution transmission microscopy (HRTEM) have been used to study the properties of Pt, Ru and Pt/Ru nano-particles. The TEM studies suggest a face centered cubic and a hcp structure for the mono-metallic Pt and Ru, respectively particles, while fcc Pt–Ru alloy formation is suggested for the Pt/Ru particles. This indicates that not all of the Ru is dissolved in the fcc Pt lattice, confirming previous views of these Pt/Ru nano-sized catalyst particles [9].

The behaviour of CO adsorbed on the nano-particle surfaces was studied using IR spectroscopy in order to obtain

information about the nano-particle surfaces. The results presented in this paper demonstrate that IR is indeed a useful technique to study bi-metallic Pt/Ru nano-particles. It was found that the stretching frequency of CO_{ads} strongly depends on the particle size and composition. First, the preparation and IR characterization of the mono-metallic Pt and Ru-colloids was demonstrated. Strong IR bands due to the stretching vibration of CO_{ads} are observed between 2010 and 2050 cm^{-1} for the Pt particles, while two bands for linear bonded CO_{ads} and, at lower wavenumbers for bridged bonded CO_{ads}, are found for the Ru particles. The band position is influenced by the particle size. In general, a frequency downshift is observed with decreasing particle size for the mono-metallic Pt and Ru nano-particles. In the case of the Pt nano-particles, mainly CO adsorbed on edge sites is observed, while essentially no CO adsorbed on terrace sites is found. This behaviour is consistent with previous observations for Pt nano-particles [23].

Differences in the band position for CO_{ads} on Pt and Ru phases are shown to allow the interpretation of the more complex spectra observed for the bi-metallic Pt/Ru nano-particles. For the larger particles ($>2 \pm 0.5$ nm), two intensities are observed in the range of around 1970 and 2050 cm^{-1}, while decreasing the particle size leads to the appearance of a third peak at $\sim$2020 cm^{-1}. The "new" band in the 2050 cm^{-1} range is assigned to CO_{ads} on Pt–Ru step sites, i.e., Pt–Ru alloy sites, while the bands in the 1970 and 2020 cm^{-1} range indicate CO_{ads} on Ru and Pt, respectively, sites. The intensities of both band characteristics for CO_{ads} on Ru and Pt increase relative to the intensity of the CO_{ads} band for the Pt–Ru alloy. The larger particles are hence believed to consist of Pt–Ru alloy and a separate Ru phase, while the number of atoms contributing to the Pt–Ru alloy phase decreases relative to the number of atoms in the Pt and Ru phase for the smaller particles.

Acknowledgements

References

[1] G. Schmid (Ed.), Clusters and Colloids, from Theory to Applications, VCH, Weinheim, 1994.
[2] C. Bock, B. MacDougall, H. Halverson, in: Y. Lin, H.S. Nalwa (Eds.), Handbook of Electrochemical Nanotechnology, American Scientific Publishers, submitted for publication.
[3] M. Watanabe, S. Motoo, J. Electroanal. Chem. 7 (1975) 428.
[4] S. Mukerjee, J. McBreen, J. Electroanal. Chem. 448 (1998) 163.
[5] A. Giroir-Fendler, D. Richard, P. Gallezot, Faraday Discuss. 92 (1991) 69.
[6] T.J. Schmidt, M. Noeske, H.A. Gasteiger, R.J. Behm, P. Britz, W. Brijoux, H. Bönnemann, Langmuir 13 (1997) 25.
[7] C. Pan, F. Dassenoy, M.-J. Casanove, K. Philippot, C. Amiens, P. Lecante, A. Mosset, B. Chaudret, J. Phys. Chem. 103 (1999) 10098.
[8] L. Dubeau, C. Coutanceau, E. Garnier, J.M. Leger, C. Lamy, J. Appl. Electrochem. 33 (2003) 419.
[9] C. Bock, C. Paquet, M. Couillard, G.A. Botton, B.R. MacDougall, J. Am. Chem. Soc. 126 (2004) 8028.
[10] R.M. Lain, A. Sellinger, United States Patent, 6, 551, 960 B1, 2003.
[11] Y. Wang, J. Ren, K. Deng, L. Gui, Y. Tang, Chem. Mater. 12 (2000) 1622.
[12] F. Dassenoy, M.-J. Casanove, P. Lecante, C. Pan, K. Philippot, C. Amiens, B. Chaudret, Phys. Rev. B 63 (2001) 235407.
[13] P.K. Babu, H.S. Kim, S.T. Kuk, J.H. Chung, E. Oldfield, A. Wieckowski, E.S. Smotkin, J. Phys. Chem. B. 36 (2005) 17192.
[14] N. Sheppard, T.T. Ngyuyen, Adv. Infrared Raman Spectrosc. (1978) 67.
[15] K.A. Friedrich, F. Henglein, U. Stimming, W. Unkauf, Electrochim. Acta 47 (2001) 689.
[16] D. deCaro, J.S. Bradley, Langmuir 13 (1997) 3067.
[17] G.L. Haller, D.E. Resasco, Adv. Catal. 36 (1989) 173.
[18] V.S. Bagotsky, Y.B. Vassiliev, Electrochim. Acta 12 (1967) 1323.
[19] S. Hadzi-Jordanov, H. Angerstein-Kozlowska, B.E. Conway, J. Electroanal. Chem. 60 (1975) 359.
[20] S. Weissmann (Ed.), Data Book, first ed., Metals & Alloys, vol. 1, Center for diffraction data JCPDS, Pensylvania, USA, 1981.
[21] M.S. Nashner, A.I. Frenkel, D.L. Adler, J.R. Shapley, R.G. Nuzzo, J. Am. Chem. Soc. 120 (1998) 8093.
[22] S.-W. Wang, L.M. Falicov, A.W. Searcy, Surf. Sci. 143 (1984) 609.
[23] S. Park, S.A. Wasileski, M.J. Weaver, J. Phys. Chem. B 105 (2001) 9719.
[24] S.-C. Chang, M.J. Weaver, J. Phys. Chem. 95 (1991) 5391.
[25] A. Schlapka, U. Käsberger, D. Menzel, P. Jakob, Surf. Sci. 502–503 (2002) 129.
[26] M. Kobayashi, T. Shirasaki, J. Catal. 28 (1973) 289.
[27] A. Duteil, R. Quéau, B. Chaudret, R. Mazel, C. Roucau, J.S. Bradley, Chem. Mater. 5 (1993) 341.
[28] J.E. Hulse, M. Moskovits, Surf. Sci. 57 (1976) 125.
[29] M. Moskovits, J.E. Hulse, Surf. Sci. 61 (1976) 302.